



Study of a nested neutron-focusing supermirror system for small-angle neutron scattering

Huarui Wu^{a,b}, Yang Yang^c, Daniel S. Hussey^d, Zhiyuan Wang^{a,b}, Kun Song^{a,b}, Zhong Zhang^{c,*}, Zhanshan Wang^c, Zhe Wang^{a,b}, Xuewu Wang^{a,b,**}

^a Department of Engineering Physics, Tsinghua University, Beijing 100084, China

^b Key Laboratory of Particle Radiation Imaging (Tsinghua University), Ministry of Education, Beijing 100084, China

^c School of Physics Science and Engineering, Tongji University, Shanghai 200092, China

^d Physical Measurement Laboratory, NIST, Gaithersburg, Maryland 20899-8461, USA

ARTICLE INFO

Keywords:

Neutron optics
SANS
Supermirror

ABSTRACT

Neutron current is crucial for neutron scattering measurements, especially for those at compact sources. Among various neutron optical devices, neutron-focusing mirrors have been drawing increasing attention due to their great potential in enhancing neutron current on sample for small-angle neutron scattering instruments. The state-of-the-art neutron-focusing mirrors, which can collect a large divergence of neutron beam, are required to be nestable and simultaneously be able to be coated with supermirrors. In this paper, we employ the nested conical optics to manufacture nested neutron-focusing mirrors with supermirror coatings. This technique enables such mirrors by assembling partial cylindrical glass segments into nested shells. A prototype system, containing two shell conical mirrors with $m=2$ Ni/Ti supermirror coatings, has been designed and manufactured. Ray-tracing simulations and neutron beam experiments have been carried out to evaluate its focusing performance and neutron reflectivity. The results show that neutron current collected by this prototype system is about 26 times higher than that by a pinhole design with the same Q_{\min} . Moreover, we discuss some possible further improvements on the fabrication process.

1. Introduction

Small-angle neutron scattering (SANS) is a well-established method for the characterization of structures of numerous substances from nano-scale to meso-scale. Quite a few neutron sources, including the state-of-the-art facilities and university-based compact sources, have been constructed to meet the growing demands for neutron beam from various research fields. Traditionally, the pinhole collimation is used in most SANS instruments. It employs a very long flight path and small tapered apertures [1], which results in a relatively weak neutron current on sample. The problem could be even severe for the instruments built at compact sources.

In an effort to enhance the scattering signal, reflective neutron-focusing mirrors have been proposed long ago to revolutionize SANS instruments [2–4]. The ultimate neutron-focusing mirrors are expected to have two features. Firstly, they should achieve a two-dimensional focusing with low aberrations such that the focusing SANS can have a small minimum accessible scattering vector Q_{\min} . This can be realized with ellipsoidal mirrors or Wolter mirrors [5,6]. Secondly, they should have a large effective collecting area for increasing the neutron current.

The effective collecting area is defined as the product of the geometric collecting area and the reflectivity of the mirrors. A prominent way to boost the geometric collecting area without introducing extra aberrations is nesting multiple confocal mirrors with full figures of rotation [5]. Upon increasing the size of the outer mirrors, the grazing angle will increase accordingly, which requires a higher critical angle to totally reflect incident neutrons. Supermirrors are routinely used to increase the critical angle for total reflection by a factor of m compared with that of pure nickel. They can be deposited on the interiors of mirrors to collect a larger divergence of neutron beam.

Recently, several fabrication methods have been reported to manufacture two-dimensional neutron-focusing mirrors. However, mirrors that can be nested and simultaneously be coated with supermirrors have not been realized. For example, Gubarev et al. [7,8] adopted electroformed nickel replication method to fabricate nested full-shell mirrors, but depositing multilayers on the interiors of full-shell mirrors is still challenging. Hosobata et al. [9] introduced a cage-like octadecagonal holder to assemble partial ellipsoidal segments into a full-shell ellipsoid. Techniques to deposit supermirrors on partial ellipsoidal segments have been established [10–12]. Nevertheless, it is still

* Corresponding author.

** Corresponding author at: Department of Engineering Physics, Tsinghua University, Beijing 100084, China.

E-mail addresses: zhangzhongcc@tongji.edu.cn (Z. Zhang), wangxuewu@tsinghua.edu.cn (X. Wang).

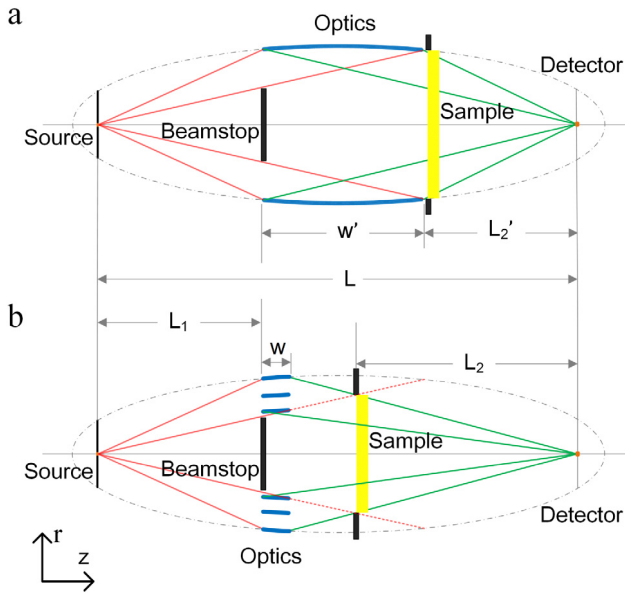


Fig. 1. Schematic view of SANS instruments with (a) a single-shell ellipsoidal mirror and (b) nested ellipsoidal mirrors. These two optics cover an equal solid angle as indicated by the red lines. The sizes of the sources are assumed to be enough small for simplicity. L_1 is the source-to-optics distance (SOD) and L is the instrument length denoting the distance from source to detector. w' and w represent the lengths of the two optics. L_2' and L_2 are the sample-to-detector distances (SDDs) in the two cases. It can be concluded from this figure that $L_2 > L_2'$. (For interpretation of the references to color in this figure legend, the reader is referred to the web version of this article.)

unrealistic to assemble multiple-shell mirrors with the current holder design.

In this study, we apply nested conical optics to manufacture nested supermirror-coated mirrors. This technique was originally developed for the fabrication of X-ray telescopes, such as the X-ray Timing and Polarization (XTP) satellite [13–15] and the Nuclear Spectroscopy Telescope Array (NuSTAR) [16,17]. The mirror substrate is cylindrically shaped glass produced by slumping commercially-available thin glass sheets. Multilayers are deposited on the glass segments that are subsequently assembled azimuthally to form a full conical shell by graphite spacers and epoxy. Conical shells with different diameters can further be nested with the support of the graphite spacers.

The nested conical optics makes the fabrication of nested supermirror-coated neutron-focusing mirrors realizable. This will be of particular importance for the neutron instruments at compact neutron sources, since this technique can dramatically enhance the neutron current. In this paper, we report the design and experimental test of a two-shell nested neutron-focusing supermirror system produced by this technique. We start by introducing the advantage and principle of the nested mirrors, and then elaborate the design of the nested supermirror system for a SANS instrument. Next, the focusing performance and the supermirror reflectivity of the system will be presented to demonstrate its capability.

2. Design of nested neutron-focusing mirrors for SANS

It is known that Wolter mirror is able to reduce the optical aberrations through double reflections [8,18]. Nevertheless, to mitigate the difficulty in manufacture and alignment, here we adopt ellipsoidal geometry that is based on single reflections. The principle of focusing with a single-shell ellipsoidal mirror has been studied by previous work [2,4,18–20]. Fig. 1(a) shows the use of a single-shell ellipsoidal mirror in a SANS instrument under grazing-incidence condition, where the source and the detector are placed at the two foci of the ellipsoid. Magnification, defined as the ratio between the size of the focal spot

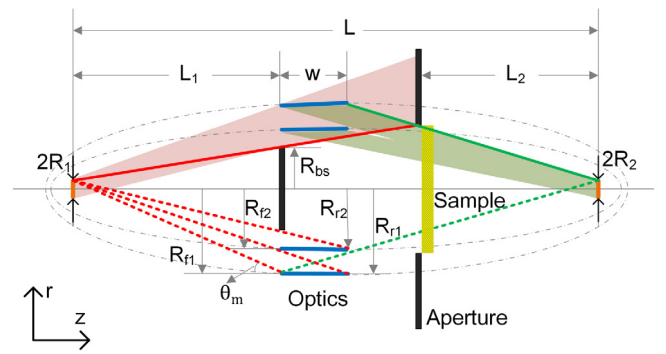


Fig. 2. Schematic of nested neutron-focusing mirrors for SANS. The illustrated optics contains two-shell ellipsoidal mirrors of which the front-end radius and the rear-end radius are denoted as R_{fi} and R_{ri} ($i = 1, 2$). A beamstop with a radius of R_{bs} is used to block the center of the optics. The neutron source is a circle with a radius of R_1 . The optics images the source onto the detector plane forming a spot with a radius of R_2 . The red lines and the red shaded area represent the incident beams, while the green ones represent the reflected beams. (For interpretation of the references to color in this figure legend, the reader is referred to the web version of this article.)

and the size of the source, is independent of the radius of mirrors, and is expressed as $M = (L - L_1)/L_1$ [20]. Therefore a circular source with a radius of R_1 will result in a focusing spot with a radius of $R_2 = MR_1$. Multiple confocal ellipsoidal mirrors can be nested with the size of the focusing spot unchanged. The size of the spot determines the minimum accessible scattering vector Q_{min} which is written as:

$$Q_{min} \cong k \frac{R_2}{SDD} \quad (1)$$

where k is the neutron wave vector and SDD represents the sample-to-detector distance.

Q_{min} and the neutron current on sample $I(n/s)$ are key figures for a SANS instrument [21]. In focusing configuration, I is proportional to the geometric collecting area of the optics. The single-shell mirror in Fig. 1(a) and the nested mirrors in Fig. 1(b) are equal in geometric collecting areas, but, L_2 in Fig. 1(b) is distinctly larger than L_2' in Fig. 1(a), which implies the nested mirror system can achieve a smaller Q_{min} . Therefore, we adopt the nested ellipsoidal geometry in this study, and the principle of the focusing with nested mirrors and their optimization strategy are presented below.

2.1. Optimization of nested neutron-focusing mirrors

The parameters of a SANS instrument with nested mirrors should be optimized for optimal performance. Although one can employ ray-tracing simulations to conduct optimization by scanning the parameters [6,22], such method based on simulations alone will consume massive amounts of computing power and time to pinpoint the optimal parameters. Here, we propose an optimization strategy based on the method of Lagrange multiplier [23] by building the connections between the design parameters of a focusing instrument and its performance.

The design parameters of a SANS instrument with nested mirrors mainly include: radius of the source aperture R_1 , source-to-detector distance L , source-to-optics distance L_1 , radius of the outermost shell R_{f1} , shell number of the nested mirrors N , length of each mirror shell w , and supermirror index m .

Without loss of generality, we set $N = 2$ to elaborate the optimization process. The schematic view of the optics with two shell mirrors is shown in Fig. 2. The radius of the inner shell R_{f2} and the radius of the beamstop R_{bs} are derived from R_1 , L , L_1 , R_{f1} and w with the following principles. Firstly, the nesting should prevent the inner shell

or the beamstop from projecting a shadow on their outer ones, which gives:

$$\frac{R_{r1} + R_1}{L_1 + w} \geq \frac{R_{r2} + R_1}{L_1} \quad (2)$$

$$\frac{R_{r2} + R_1}{L_1 + w} \geq \frac{R_{bs} + R_1}{L_1} \quad (3)$$

where R_{fi} and R_{ri} ($i = 1, 2$) satisfy the equation of an ellipse. In addition, the beam reflected by the outer shell should avoid intersecting with the inner shell:

$$\frac{R_{f1} + MR_1}{L - L_1} \geq \frac{R_{r2} + MR_1}{L - L_1 - w} \quad (4)$$

With Eqs. (2)–(4), the parameters of the nested shells can be obtained from the design parameters. Next, we elaborate the optimization strategy by expressing the instrument performance as a function of the design parameters.

Eq. (1) connects Q_{\min} and the design parameters. R_2 is simply equal to MR_1 , while the maximum SDD is limited by more parameters. To prevent the unreflected neutrons illuminating the sample, the sample should be placed beyond the red shaded area in Fig. 2. Therefore the maximum SDD is achieved by putting the sample on the intersection point of the red and green solid lines. It is written as:

$$L_2 = \frac{\frac{L}{L_1} R_{bs} - (\frac{L-L_1}{L_1} + \frac{L-L_1-w}{L_1+w}) R_1}{\frac{1}{L_1} R_{bs} + \frac{1}{L-L_1-w} R_{r1} - (\frac{1}{L_1} + \frac{1}{L_1+w}) R_1} \quad (5)$$

For $w \ll L$, it can be simplified to:

$$L_2 = \frac{R_{bs} - 2\frac{M}{M+1} R_1}{R_{bs} + \frac{R_{f1}}{M} - 2R_1} L \quad (6)$$

Hence,

$$Q_{\min} = \frac{kMR_1}{L_2} = \frac{kR_1}{L} \frac{R_{bs} + \frac{R_{f1}}{M} - 2R_1}{\frac{R_{bs}}{M} - \frac{2R_1}{M+1}} \quad (7)$$

In the case of an isotropic source, the neutron current on sample is proportional to the source area and the geometric collecting area of the nested mirrors.

$$I = I_0 \cdot \pi R_1^2 \cdot \frac{\pi(R_{f1}^2 - R_{bs}^2)}{L_1^2} \quad (8)$$

where I_0 incorporates the source brightness and the reflectivity of the mirrors.

The supermirror index, m , adds a constraint to the maximum size of the mirrors. To reflect all neutrons with wavelength larger than λ_c , the maximum grazing-incidence angle θ_m should be lower than the critical angle θ_c that is a function of λ_c and m . This constraint is written as:

$$\theta_m = \frac{1}{2}(\pi - \arctan \frac{L_1}{R_{f1} + R_1} - \arctan \frac{L - L_1}{R_{f1} + MR_1}) \leq \theta_c(\lambda_c, m) \quad (9)$$

With the above relations, Lagrange multiplier method can be employed to maximize I/Q_{\min} with different given conditions. It is noted that this optimization process is based on some approximations and simplifications. The exact optimal parameters should be further obtained by ray-tracing simulations. Notwithstanding this, the proposed strategy can bring a better understanding on the instrument design and greatly narrow the ranges of the optimal parameters.

2.2. Design of the prototype nested supermirror system

We apply the optimization strategy to design a prototype system which will be installed on the SANS beamline of the Compact Pulsed Hadron Source (CPHS) [24] and will offer an optional configuration compatible with the previous pinhole design [25]. With considerations of the engineering aspects, these two configurations will share collimation and detector system. Consequently, the optimization of the mirrors

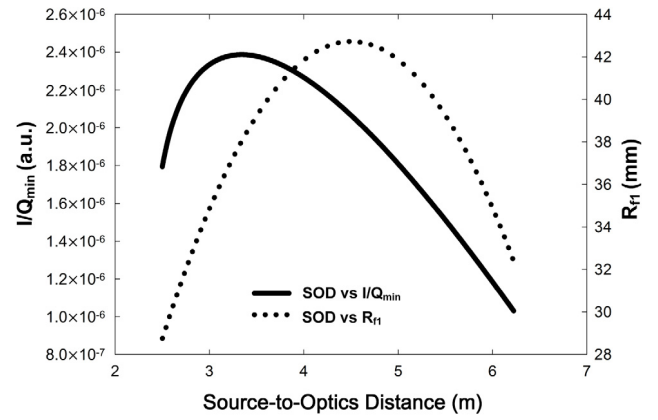


Fig. 3. The optimal R_{r1} (the dotted line) and the corresponding I/Q_{\min} (the solid line) vs SOD. For each SOD, the optimal R_{r1} leading to largest possible I/Q_{\min} is calculated. The optimization was implemented with the following constraints: $R_1=14$ mm, $m=2$, $\lambda_c=4$ Å, $L=8$ m, $w=0.2$ m, and the number of nested shells is two.

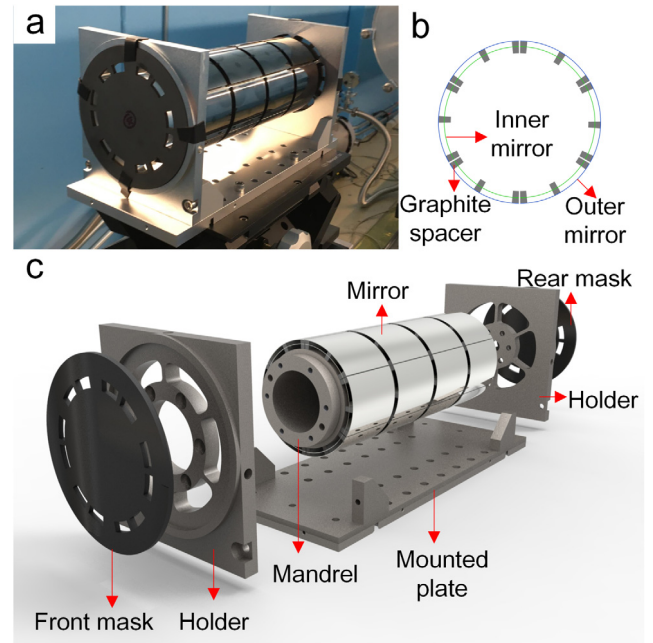


Fig. 4. The nested neutron-focusing supermirror system. (a) Photograph of the prototype system. (b) Schematic view of the azimuthal structure. The device contains two shell mirrors, each of which is azimuthally divided into six segments. Graphite spacers are employed to support mirror segments. (c) Exploded view of the prototype system. It contains four axial conical segments. The masks are used to prevent neutrons hitting the graphite spacers or directly reaching detector.

is implemented with $R_1 = 14$ mm and $L = 8.0$ m as in the pinhole configuration. In addition, as a proof of technology, the nested shell number of the prototype system was set to two and the coatings were chosen to be $m=2$ Ni/Ti supermirrors to ease the fabrication. Extra restrictions were added by the fabrication technique and the assembly process: the length of each glass segment is 5 cm, meanwhile the total length of each shell is less than about 20 cm. Thereupon, four 5 cm segments are employed to approximate the ellipsoidal geometry.

With the above constraints, the aforementioned optimization strategy was carried out to find L_1 and the size of the mirrors. Fig. 3 shows the optimal R_{r1} and the corresponding I/Q_{\min} as a function of L_1 . After peaking at $L_1=3.3$ m, I/Q_{\min} drops steadily. Due to the shielding and collimation arrangement of CPHS, the accessible L_1 has to be larger than 4.8925 m to accommodate the nested supermirror

Table 1
Design parameters of the nested mirrors.

Focal length L (mm)	8000.0
Source-to-optics distance L_1 (mm)	4892.5
Outer shell radius R_{r1} (mm)	42.44
Inner shell radius R_{r2} (mm)	39.12
Length of axial segments (mm)	50
Number of axial segments	4
Number of azimuthal segments	6
Substrate	0.3-mm-thick glass
Coating	$m = 2$ Ni/Ti supermirror

system. With Eqs. (2)–(4) and additional ray-tracing simulations, the design parameters are specified and listed in Table 1.

The nested supermirror system has been fabricated with the nested conical optics and it is shown in Fig. 4. The supermirror structure containing 40 bilayers was designed with the ABC method [26]. DC magnetron sputtering was employed to coat Ni/Ti bilayers on the cylindrical glass substrate. The prototype system is divided into four axial segments and six azimuthal segments, thus it consists 48 mirror segments. To build up these segments into nested shells, graphite spacers were epoxied axially along the mandrel, as well as azimuthally around the mandrel. Each mirror segment is supported by three graphite rods. Boron carbide masks are placed before and after the mirrors to prevent neutrons hitting the graphite spacers and the mandrel. The use of mask is essential but will drastically reduce the geometric collecting area to about 60% of the ideal one. Though the nested conical optics cannot produce the true full-figure rotation mirrors, its capability to nest multiple shells can significantly enlarge the geometric collecting area.

2.3. Simulation evaluations of the design

Ray-tracing simulations have been carried out to evaluate the performance of the nested supermirror system with the help of McStas package [27]. In McStas, neutron beams are treated as rays of geometrical optics. The interaction of neutrons and supermirrors is described by a reflectivity function. The reflectivity of the $m = 2$ supermirrors is represented by Heaviside step function in terms of Q , which is equal to zero for Q larger than the critical value Q_c and otherwise one.

Taking the mirror geometry and the reflectivity function as the input of McStas, the reflectivity responses of the two shell mirrors to different neutron wavelengths are obtained respectively. They are expressed as reflectivity functions in terms of wavelength, which are shown in Fig. 5. The results are in line with our expectations that all cold neutrons with wavelength larger than 4 \AA can be totally reflected by the mirrors. A cutoff wavelength exists at about $\lambda = 2.4 \text{ \AA}$ below which the reflectivity approaches zero. This cutoff effect can avoid fast neutrons arriving at the detector and is particularly useful to accelerator-driven neutron sources since fast neutron is one of the main sources of background [28,29].

To investigate the effect of the conical approximation, the magnifications of perfect ellipsoidal mirrors and the conical mirrors are calculated by simulations and are compared in Fig. 6. The conical approximation introduces extra slope errors. Consequently, it enlarges the focusing spots and deteriorates Q -resolution. The increment in the radius of the focusing spot is about half millimeter in our design. Compared with the typical spatial resolution of the SANS detectors and the size of the source apertures, the deterioration in Q -resolution is neglectable. For the applications in high-resolution instruments, smaller spots can be obtained by employing shorter conical segments to approach the ellipsoidal geometry where coma is the dominant aberration [30], or with a double-reflection geometry [18].

The geometric collecting area of the prototype system is evaluated to be about 624 mm^2 by simulations, with the masks' effect taken into consideration. This quantity is much larger than the typical size of the

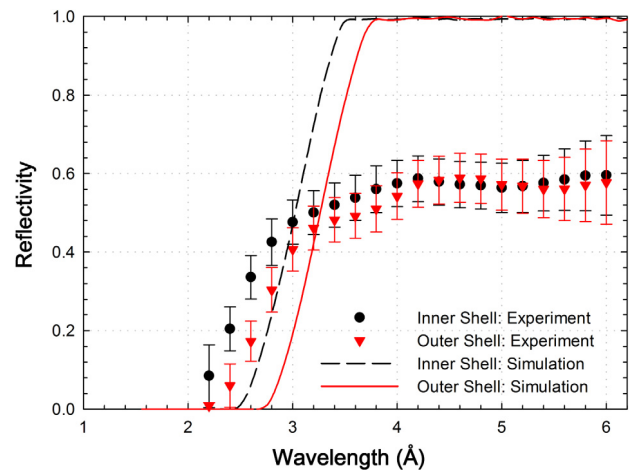


Fig. 5. Neutron reflectivity of the two shell mirrors as a function of wavelength. The simulation results were obtained by McStas, assuming that the coatings are perfect $m = 2$ supermirrors. The experimental results are discussed in Section 3.

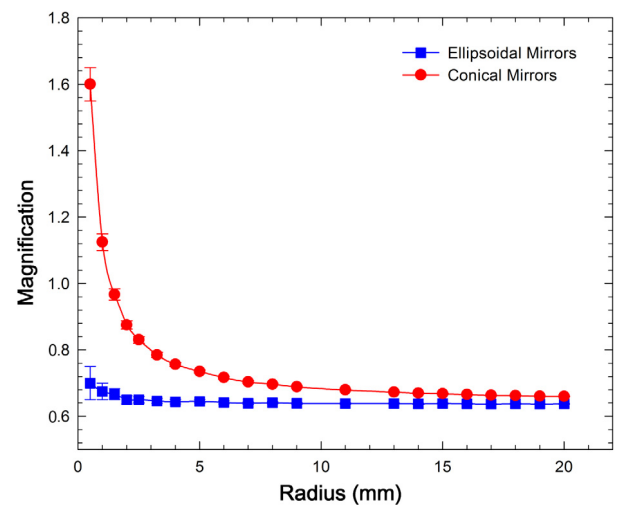


Fig. 6. The magnification of the perfect ellipsoidal mirrors and the designed conical mirrors as a function of source radius. The upturn occurred at small radius is due to the optical aberrations. The deviations between the two geometries are attributed to the slope errors of conical approximation.

sample apertures of pinhole setup. Fig. 7 compares the radial profiles of the spots on detector obtained by the nested neutron-focusing mirrors and the pinhole collimator, respectively. According to Eq. (5), the maximum SDD of the focusing setup is about 2.6 m while the SDD of the pinhole setup for CPHS is 3.0 m. Though the focusing setup lacks in SDD, its source area and geometric collecting area compensate for that. With the same Q_{\min}/k equal to 3.6×10^{-3} rad, the neutron-focusing mirrors can still earn a 44-fold increase in neutron current.

3. Experimental evaluations of the prototype nested supermirror system

The prototype system was experimentally tested at the cold neutron imaging facility located at the end of NG6 neutron guide at the NIST Center for Neutron Research [31]. This facility permits a long flight path to conduct focusing experiments. Moreover, its high-resolution detector enables a careful examination on the figure accuracy of the optics.

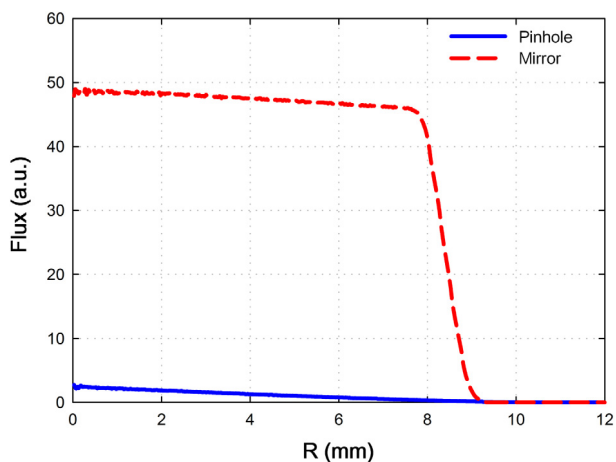


Fig. 7. Comparison of the spot profiles on detector between the neutron-focusing mirror setup and the pinhole setup. The results are obtained by performing McStas simulations. The source-to-detector distances in both setups are 8.0 m. In the focusing setup: the diameter of the source aperture is 28.00 mm, SDD is 2.6 m, and the diameter of the focusing spot is 18.70 mm. In the pinhole setup: the diameter of the source aperture is 17.98 mm, the diameter of the sample aperture located at 5.0 m from the source aperture is 6.74 mm, SDD is 3.0 m, and the diameter of the direct spot is 21.58 mm. With the above arrangements, the two configurations can achieve the same Q_{min}/k making the comparison impartial.

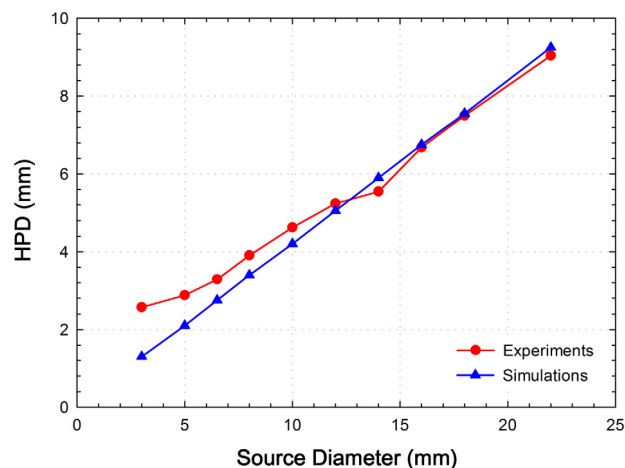


Fig. 9. HPD as a function of source diameter.

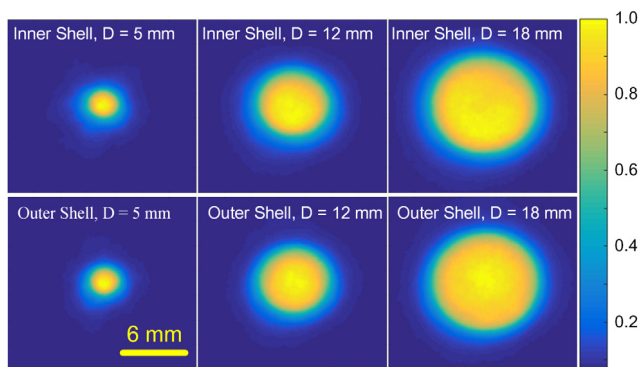


Fig. 8. Images of the focusing spots. The contrast has been normalized to the highest counts.

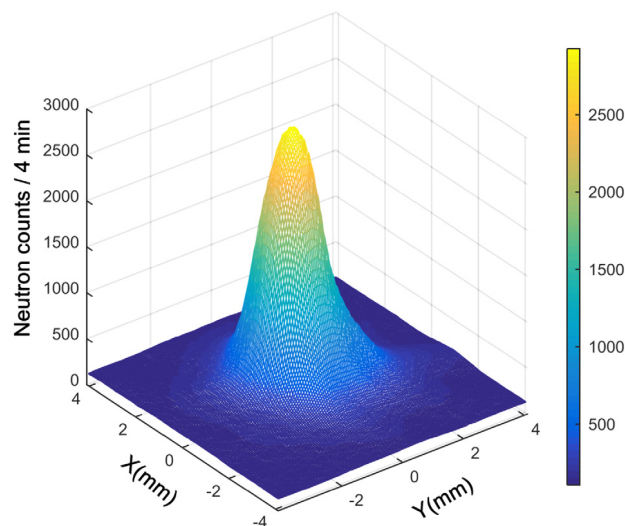


Fig. 10. 3D view of the focusing spot of the 3-mm-diameter source.

3.1. Focusing performance of the nested supermirror system

In the focusing experiment, 5 Å neutrons were selected by the highly oriented pyrolytic graphite (HOPG), and a scintillator detector with a spatial resolution of about 150 μm was used to record the focused images. The source aperture and the detector were placed at the two foci of the mirrors and were aligned with laser and neutron beams before the final measurements. A 3.2-m-long fight tube was placed between the optics and the source aperture. The inner shell mirror and the outer shell mirror were tested successively by putting the dedicated boron cable masks at the two ends of the optics.

Fig. 8 shows the focused images acquired with varied source diameters. The image centers were calculated as the flux-weighted average position to evaluate the coaxiality of the inner and outer shells. A 0.2 mm separation was found between the centers of the images formed by the two shells. This separation will not bring perceptible deterioration to the instrument performance. The intensity distributions of the spots exhibit a slight nonuniformity, which implies that some of the mirror segments were not installed correctly or have a lower figure accuracy.

High-power diameter (HPD) is used to characterize the focusing quality of the ensemble system. In contrast to magnification, HPD does

not require an accurate determination of the spot boundary. The measured HPD of the spots obtained by the outer shell and the inner shell coincide, and thus only one experimental curve is plotted and compared with the simulation results in Fig. 9. The measured HPD increases with the source diameter which demonstrates the magnifying capability of the mirrors. The consistency between the experimental curve and the simulation curve manifests the overall quality of the focusing system. The smallest source diameter measured in our experiment was 3 mm, corresponding to a measured HPD of 2.5 mm. Therefore, we conclude that the resolution of the prototype system is better than 2.5 mm. The 3D view of the smallest focusing spot is displayed in Fig. 10. A slowly decayed tail is perceived in the edge of the spot, which may be caused by diffuse scattering by the mirrors and other parasitic scattering by apertures, air and aluminium windows. The effect of diffuse scattering on the SANS performance has been discussed a lot [3,32]. However, we did not carry out a quantitative analysis on it due to the high noise.

3.2. Reflectivity measurement of the curved supermirrors

Reflectivity function in terms of Q is often used to evaluate the quality of supermirrors. Whereas for curved supermirrors, the incident angle varies with reflecting points on the mirror surface. An accurate determination of the incident angle requires a highly-collimated beam,

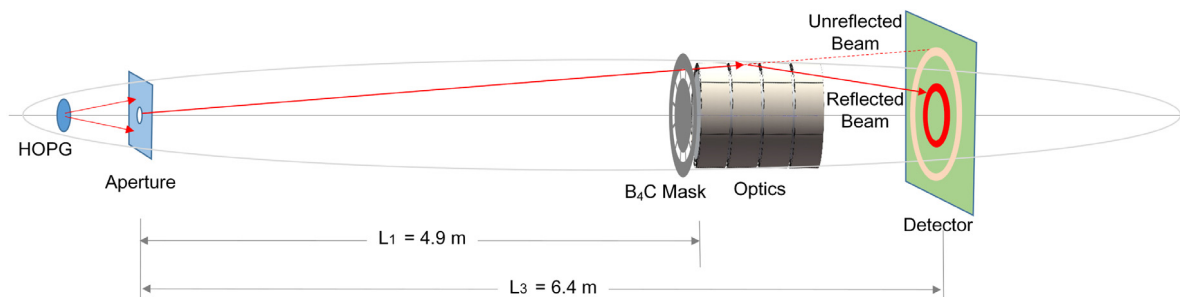


Fig. 11. Schematic drawing of the experimental setup.

which currently is rather challenging. In this study, the reflectivity of the mirrors is measured as a function of wavelength λ , which can also offer an examination on the supermirror quality. Neutron wavelengths ranging from 2.2 Å to 6.0 Å were monochromatically selected by HOPG for the measurements.

The effective collecting area $A(\lambda)$ is introduced to incorporate the effect of reflectivity on the reflected neutron current. It is defined as the product of the geometric collecting area A_g and the supermirror reflectivity $R(\lambda)$. $A(\lambda)$ is experimentally measured as the ratio of the reflected current $I_f(\lambda)$ (n/s) to the incident flux $F_i(\lambda)$ (n/s/mm²) at the optics position. Hence, $R(\lambda)$ is given by:

$$R(\lambda) = \frac{A(\lambda)}{A_g} = \frac{I_f(\lambda)}{F_i(\lambda)A_g} \quad (10)$$

Fig. 11 illustrates the experimental layout of the reflectivity measurements. F_i was not directly measured by moving the detector to the optics position but was calculated as $F_i(\lambda) = F_r(\lambda)L_3^2/L_1^2$, where L_1 and L_3 are denoted in Fig. 11 and $F_r(\lambda)$ is the direct beam flux at $z = L_3$ with the mirrors removed. The detector sitting at $z = L_3$ successively measured $I_f(\lambda)$ and $F_r(\lambda)$ with the mirrors on and off the beamline.

The reflectivity measurements were taken respectively for the inner shell and the outer shell, and the results are shown in Fig. 5. The background of each measurement has been subtracted and the measurement errors were calculated with considerations on the background and the detection efficiency. At short wavelengths, the measured reflectivity is higher than the simulation reflectivity of the ideal $m=2$ supermirrors. As mentioned above, the reflectivity in terms of Q of a real supermirror is not zero for $Q > Q_c$, which accounts for that the measured reflectivity at short wavelengths is higher. Besides, the inner shell outperforms the outer shell in short-wavelength reflectivity, which can be explained by the geometrical course that the smaller radius of the inner shell leads to a smaller grazing angle. The reflectivity at longer wavelengths plateaus at 60%. Therefore, the effective collecting area of $\lambda = 4\text{--}6$ Å is about 374 mm², which corresponds to a 26-fold neutron current increase compared with the pinhole design with the same Q_{\min}/k .

One should note that the grazing-incidence angle ranges from 0.48° to 0.75°. Even for the longest wavelength measured here, the grazing-incidence angles of the most incident neutrons are beyond the critical angle of nickel, which suggests that the degradation in reflectivity is largely due to the imperfections at Q from $m=1$ to $m=2$ but not at $m < 1$. To investigate the supermirror structure, a flat sample coated with the same supermirror under the same deposition process but on a flat glass substrate was fabricated, and its structure was investigated by cross-sectional observations using a transmission electron microscopy (TEM). The TEM results showed that the poorest local interfacial roughness is up to 2.3 nm, which suggests that roughness is one of the main causes of the reflectivity deterioration [33]. Besides that, non-uniform deposition on cylindrical substrates and mid-spatial frequency variations may also contribute to the deterioration. More investigations are required to confirm them, and further efforts are underway to improve the supermirror quality by refining the deposition technique and adopting other materials such as NiC/Ti that has proved to be superior to Ni/Ti [34].

4. Conclusions

In this work, we perform a comprehensive investigation on a nested supermirror system that is developed to enhance the neutron current for SANS instruments. This system is based on the nested conical optics, which is able to simultaneously realize the nested structure and the supermirror coating. We propose an optimization strategy for nested mirrors. Following this strategy, we design and fabricate a prototype system containing two-shell conical mirrors. Neutron-focusing experiments have been carried out to evaluate the figure quality of the system. It is found that its resolution is better than 2.5 mm. We also measure the reflectivity of the system as a function of neutron wavelength. The result shows that the peak reflectivity is about 60%, which results in an effective collecting area of 374 mm² and a 26-fold gain in neutron current compared with the pinhole design with the same Q_{\min}/k . These results suggest that nested supermirror system produced by the technique is promising to improve the performance of SANS at compact sources. Further improvements, especially on the supermirror deposition process, are under development in our labs.

Acknowledgments

The authors would like to express their grateful thanks to the support of the National Institute of Standards and Technology, U.S. Department of Commerce, in providing the neutron research facilities used in this work. Preliminary experiments were performed at the China Spallation Neutron Source and the China Mianyang Research Reactor. H.W. is grateful for helpful discussions with Dr. Boris Khaykovich of MIT and Jiewei Shen of RUC. This work was supported by the National Natural Science Foundation of China (grant No. 11275106 and No. 11322548).

References

- [1] J.S. Higgins, H.C. Benoit, *Polymers and Neutron Scattering*, Oxford science publications, 1994.
- [2] B. Alefeld, H. Fabian, T. Springer, Recent studies in neutron optics, in particular for small-angle neutron scattering, in: *Thin Film Neutron Optical Devices: Mirrors, Supermirrors, Multilayer Monochromators, Polarizers, and Beam Guides*, Vol. 983, International Society for Optics and Photonics, 1989, pp. 120–129.
- [3] B. Alefeld, D. Schwahn, T. Springer, New developments of small angle neutron scattering instruments with focussing, *Nucl. Instrum. Methods Phys. Res. A* 274 (1–2) (1989) 210–216.
- [4] C. Majkrzak, C. Glinka, S. Sattja, Applications of mirrors, supermirrors and multilayers at the national bureau of standards cold neutron research facility, in: *Thin Film Neutron Optical Devices: Mirrors, Supermirrors, Multilayer Monochromators, Polarizers, and Beam Guides*, Vol. 983, International Society for Optics and Photonics, 1989, pp. 129–144.
- [5] B. Khaykovich, M. Gubarev, Y. Bagdasarova, B. Ramsey, D. Moncton, From X-ray telescopes to neutron scattering: Using axisymmetric mirrors to focus a neutron beam, *Nucl. Instrum. Methods Phys. Res. A* 631 (1) (2011) 98–104.
- [6] D. Liu, M.V. Gubarev, G. Resta, B.D. Ramsey, D.E. Moncton, B. Khaykovich, Axisymmetric grazing-incidence focusing optics for small-angle neutron scattering, *Nucl. Instrum. Methods Phys. Res. A* 686 (2012) 145–150.
- [7] B.D. Ramsey, Replicated nickel optics for the hard-X-ray region, *Exp. Astron.* 20 (1–3) (2005) 85–92.

- [8] M. Gubarev, B.D. Ramsey, D. Engelhaupt, J.M. Burgess, D. Mildner, An evaluation of grazing-incidence optics for neutron imaging, *Nucl. Instrum. Methods Phys. Res. B* 265 (2) (2007) 626–630.
- [9] T. Hosobata, M. Hino, H. Yoshinaga, T. Kawai, H. Endo, Y. Yamagata, N.L. Yamada, S. Takeda, Precision mechanical design of 900 mm long ellipsoidal neutron-focusing supermirror for VIN ROSE at J-PARC/MLF, in: *Proceedings of the International Conference on Neutron Optics, NOP2017*, 2018, p. 011010.
- [10] J. Guo, S. Takeda, S.-y. Morita, M. Hino, T. Oda, J.-i. Kato, Y. Yamagata, M. Furusaka, New fabrication method for an ellipsoidal neutron focusing mirror with a metal substrate, *Opt. Express* 22 (20) (2014) 24666–24677.
- [11] J. Guo, Y. Yamagata, S.-y. Morita, S. Takeda, J.-i. Kato, M. Hino, M. Furusaka, Figure correction of a metallic ellipsoidal neutron focusing mirror, *Rev. Sci. Instrum.* 86 (6) (2015) 063108.
- [12] S. Takeda, Y. Yamagata, N.L. Yamada, M. Hino, T. Hosobata, J. Guo, S.-y. Morita, T. Oda, M. Furusaka, Development of a large plano-elliptical neutron-focusing supermirror with metallic substrates, *Opt. Express* 24 (12) (2016) 12478–12488.
- [13] Z. Wang, Z. Shen, B. Mu, X. Wang, X. Yang, L. Jiang, R. Qi, M. Wen, Z. Zhang, B. Ma, Development of the X-ray timing and polarization telescope optics, in: *Space Telescopes and Instrumentation 2014: Ultraviolet to Gamma Ray*, Vol. 9144, International Society for Optics and Photonics, 2014, p. 91441E.
- [14] Z. Wei, B. Ge, X. Jin, N. Liu, Y. Liao, B. Ma, Y. Bai, Z. Wang, Development of manufacture of mirror glass substrate for X-ray timing and polarization observatory, in: *Space Telescopes and Instrumentation 2016: Ultraviolet to Gamma Ray*, Vol. 9905, International Society for Optics and Photonics, 2016, p. 99057E.
- [15] Z. Shen, X. Wang, K. Wang, B. Ma, Q. Huang, Z. Zhang, H. Wang, Y. Dai, P. He, Z. Wang, Development of X-ray multilayer telescope optics for XTP mission, in: *Space Telescopes and Instrumentation 2016: Ultraviolet to Gamma Ray*, Vol. 9905, International Society for Optics and Photonics, 2016, 990520.
- [16] F.A. Harrison, W.W. Craig, F.E. Christensen, C.J. Hailey, W.W. Zhang, S.E. Boggs, D. Stern, W.R. Cook, K. Forster, P. Giommi, et al., The nuclear spectroscopic telescope array (NuSTAR) high-energy X-ray mission, *Astrophys. J.* 770 (2) (2013) 103.
- [17] W.W. Craig, H. An, K.L. Blaedel, F.E. Christensen, T.A. Decker, A. Fabricant, J. Gum, C.J. Hailey, L. Hale, C.B. Jensen, et al., Fabrication of the nustar flight optics, in: *Optics for EUV, X-Ray, and Gamma-Ray Astronomy V*, Vol. 8147, International Society for Optics and Photonics, 2011, p. 81470H.
- [18] D. Mildner, M. Gubarev, Wolter optics for neutron focusing, *Nucl. Instrum. Methods Phys. Res. A* 634 (1) (2011) S7–S11.
- [19] D. Liu, B. Khaykovich, M.V. Gubarev, J.L. Robertson, L. Crow, B.D. Ramsey, D.E. Moncton, Demonstration of a novel focusing small-angle neutron scattering instrument equipped with axisymmetric mirrors, *Nature Commun.* 4 (2013) 2556.
- [20] J.G. Barker, C.J. Glinka, Development of a focusing mirror for SANS, in: *Neutron Optical Devices and Applications*, Vol. 1738, International Society for Optics and Photonics, 1992, pp. 386–395.
- [21] K.C. Littrell, A comparison of different methods for improving flux and resolution on SANS instruments, *Nucl. Instrum. Methods Phys. Res. A* 529 (1–3) (2004) 22–27.
- [22] H. Wu, B. Khaykovich, X. Wang, D.S. Hussey, Wolter mirrors for neutron imaging, *Physics Procedia* 88 (2017) 184–189.
- [23] D.P. Bertsekas, *Constrained Optimization and Lagrange Multiplier Methods*, Academic press, 2014.
- [24] X. Wang, Q. Xing, S. Zheng, Y. Yang, H. Gong, Y. Xiao, H. Wu, Z. Wang, Z. Fang, Z. Jiang, et al., Status report on accelerator and neutron activities of CPHS at Tsinghua University, *J. Phys.: Conf. Ser.* 1021 (2018) 012006.
- [25] T. Huang, H. Gong, B. Shao, D. Wang, X. Zhang, K. Zhang, J. Wei, X. Wang, X. Guan, C.-K. Loong, et al., Design of a new time-of-flight small-angle neutron scattering instrument at CPHS, *Nucl. Instrum. Methods Phys. Res. A* 669 (2012) 14–18.
- [26] K.D. Joensen, P. Voutov, A. Szentgyorgyi, J. Roll, P. Gorenstein, P. Høghøj, F.E. Christensen, Design of grazing-incidence multilayer supermirrors for hard-X-ray reflectors, *Appl. Opt.* 34 (34) (1995) 7935–7944.
- [27] P. Willendrup, E. Farhi, K. Lefmann, Mcstas 1.7-a new version of the flexible Monte Carlo neutron scattering package, *Physica B* 350 (1–3) (2004) E735–E737.
- [28] T. Huang, H. Gong, B. Shao, J. Wei, X. Guan, C.-K. Loong, J. Tao, L. Zhou, Design of the time-of-flight small-angle-neutron scattering instrument at CPHS, *Physics Procedia* 26 (2012) 44–48.
- [29] Y. Ikeda, A. Taketani, M. Takamura, H. Sunaga, M. Kumagai, Y. Oba, Y. Otake, H. Suzuki, Prospect for application of compact accelerator-based neutron source to neutron engineering diffraction, *Nucl. Instrum. Methods Phys. Res. A* 833 (2016) 61–67.
- [30] P.M. Bentley, S.J. Kennedy, K.H. Andersen, D.M. Rodriguez, D.F. Mildner, Correction of optical aberrations in elliptic neutron guides, *Nucl. Instrum. Methods Phys. Res. A* 693 (2012) 268–275.
- [31] D.S. Hussey, C. Brocker, J. Cook, D. Jacobson, T. Gentile, W. Chen, E. Baltic, D. Baxter, J. Doskow, M. Arif, A new cold neutron imaging instrument at NIST, *Physics Procedia* 69 (2015) 48–54.
- [32] C.J. Glinka, J.G. Barker, D. Mildner, Comparison of pinhole collimation and focusing optics for SANS, *Nucl. Instrum. Methods Phys. Res. A* 795 (2015) 122–127.
- [33] S. Sinha, E. Sirota, S. Garoff, H. Stanley, X-ray and neutron scattering from rough surfaces, *Phys. Rev. B* 38 (4) (1988) 2297.
- [34] R. Maruyama, D. Yamazaki, T. Ebisawa, K. Soyama, Effect of interfacial roughness correlation on diffuse scattering intensity in a neutron supermirror, *J. Appl. Phys.* 105 (8) (2009) 083527.